CHEMISTRY OF MATERIALS

ARTICLE

pubs.acs.org/cm

Syntheses, Structures, and Magnetic and Thermoelectric Properties of Double-Tunnel Tellurides: $A_xRE_2Cu_{6-x}Te_6$ (A = K−Cs; RE = La−Nd)

Chang-Yu Meng,[†,‡] Hong Chen,[†] Peng Wang,[†,‡] and Ling Chen*[,†]

[†]Key Laboratory of Optoelectronic Materials Chemistry and Physics, Fujian Institute of Research on the Structure of Matter, Chinese Academy of Sciences, Fuzhou, Fujian 350002, People's Republic of China

[‡]Graduate School of Chinese Academy of Sciences, Beijing 100039

Supporting Information

ABSTRACT: Novel double-tunnel compounds $A_xRE_2Cu_{6-x}Te_6$ (A = K−Cs; RE = La−Nd) have been synthesized from the elemental mixtures in the ACl flux at 1123 K and crystallized in the hexagonal $P6_3/m$, with a = 9.955(3)−10.0841(6) Å, c = 4.1487(6)−4.2366(6) Å, and Z = 1. A nice reconstruction of the $CuTe_4$-based anionic network has been driven by a cationic substitution of 3 Ba^{2+} with a combination of x A^+ and 2 RE^{3+} on going from $Ba_3Cu_6Te_6$ to the title compounds. The undoped sintered polycrystalline La-, Ce-, and Pr-sample (containing 2−4% CsCl impurity) have realized the figure of merit (ZT) of 0.26 at 614 K, 0.17 and 0.23 at 660 K. Typical behaviors of a narrow gap semiconductor or a semi metal are revealed by the electrical conductivity, Seebeck coefficient measurements and the VASP calculations. The presence of the multiple minima in the conduction band and the monotonic increase of ZT with temperature indicate that further enhancement of TE property is possible.

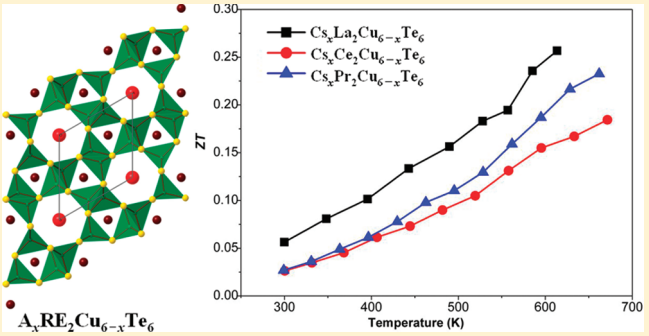

KEYWORDS: quaternary telluride, $ARE_2Cu_5Te_6$, solid state synthesis, thermoelectric

INTRODUCTION

The continuous interest on quaternary alkali (alkaline-earth)/rare earth/copper/tellurium A(AE)/RE/Cu/Te stems from not only their many potentially useful material applications but also the fascination structure characters.[1] Most of the quaternary A/RE/Cu/Te compounds are layered or tunnel structures, such as the square Te nets in $ARECuTe_4$[2,3] and $KEuCu_2Te_4$.[4,5] The tunnel structure examples are $K_{0.5}Ba_{0.5}DyCu_{1.5}Te_3$,[6] $K_3RE_4Cu_5Te_{10}$[7] as well as $CsGd_2CuTe_4$[8] and $CsSc_3Cu_2Te_6$.[9] The majority of ternary A(AE)/Cu/Te compounds contains Te−Te covalent bonds that determine/influence the physical properties.[10] Few exceptions are ACuTe (A = K, Na),[11] ACu_3Te_2 (A = K, Na),[12,13] and $Ba_3Cu_6Te_6$.[14]

Thermoelectric (TE) materials are utilized to convert thermal energy from a temperature gradient into electric energy or to convert electric energy into a temperature gradient. And the current challenge in the efforts for identifying promising TE materials lies in achieving simultaneously high electrical conductivity (σ), high Seebeck coefficient (S), and low thermal conductivity (κ) in the same material according to the dimensionless figure of merit $ZT = S^2\sigma T/\kappa$,[15] in which T is absolute temperature. Regarding TE properties, reported quaternary A(AE)/RE/Cu/Te and ternary A(AE)/Cu/Te compounds are unfortunately poor. For example, $KCeCuTe_4$ shows metallic electrical conductivity and very low Seebeck coefficient (σ_{rt} = 180 S/cm, S_{rt} = +3 μV/K).[2] Exclude the compounds with Te−Te bond, only one report on the ternary $Ba_3Cu_6Te_6$ that shows moderate electrical conductivity and relatively large Seebeck coefficient (σ_{rt} = 127 S/cm, S_{rt} = +88 μV/K) and ZT of 0.01 at room temperature,[14] and there is no report on the TE property of quaternary A(AE)/RE/Cu/Te compound.

In this paper, we discover new $A_xRE_2Cu_{6-x}Te_6$ compounds adopting a novel double-tunnel structure constructed by $CuTe_4$ tetrahedral building units. In comparison with that in $Ba_3Cu_6Te_6$,[14] such a Cu/Te framework shows a reconstruction caused by the replacement of the bivalence Ba^{2+} cation by a combination of monovalent A^+ and trivalent RE^{3+} cations. More interestingly, the primary measurements on undoped sintered polycrystalline pellets of $Cs_xRE_2Cu_{6-x}Te_6$ (with 2.5, 3.1, and 4.2% CsCl impurity for La-, Ce-, and Pr-sample, respectively) show improved thermoelectric properties that is comparable to some well-known TE compounds.[16] At room temperature, ZT values (La, 0.05; Ce, 0.02; Pr, 0.02) are higher than the 0.01 of $Ba_3Cu_6Te_6$. Furthermore, ZT values monotonically increase with temperature and realize 0.26, 0.17, and 0.23 at 614, 660, and 660 K for La-, Ce-, and Pr-sample. This distinguishes the title compounds as a new family for promising TE material candidate and further improvement of ZT value is expected.

Received: June 4, 2011
Revised: October 2, 2011
Published: October 24, 2011

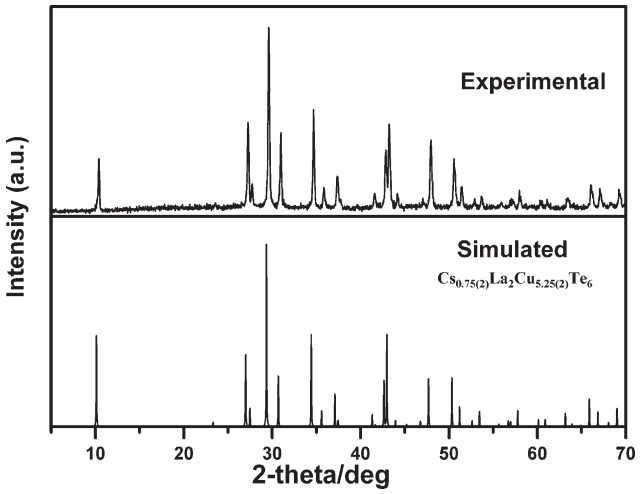

Figure 1. Experimental XRD pattern and the simulated one of $Cs_{0.75(2)}La_2Cu_{5.25(2)}Te_6$.

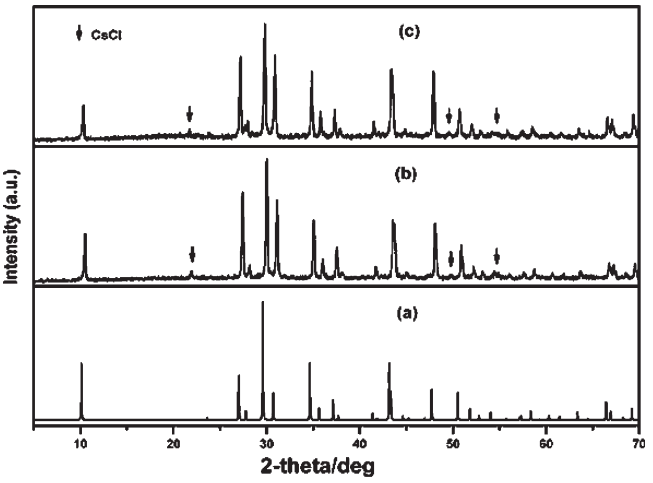

Figure 2. Simulated XRD pattern of $Cs_{0.73(4)}Pr_2Cu_{5.27(2)}Te_6$ (a) and the ones taken on the bottom part of a sintered ingot before (b) and after (c) the thermoelectric property measurements. Symbol represents CsCl phase.

EXPERIMENTAL SECTION

Syntheses of the Title Compounds. The following reactants were used as purchased and stored in a glovebox filled with purified Ar (moisture and oxygen level is less than 0.1 ppm), and all manipulations were performed inside the glovebox. Lanthanide elements (La, Ce, Pr, Nd, 99.95%) were purchased from Huhhot Jinrui Rare Earth Co., Ltd. Cu and Te with purities of 99.99% were purchased from Alfa Aesar China (Tianjin) Co., Ltd. KCl, RbCl, and CsCl with purities of 99.9% were purchased from Jiangxi Dongpeng New Materials Co., Ltd.

$A_xRE_2Cu_{6-x}Te_6$ (A = K, Rb, Cs; RE = La, Ce, Pr, Nd) were synthesized by the mixture of 3 mmol of ACl, 2.4 mmol of RE, 5 mmol of Cu and 6 mmol of Te via high temperature solid-state reactions. ACl worked as a reagent as well as a flux to assist the crystallization of the target compounds. A reaction mixture was loaded into a fused-silica tube under an Ar atmosphere in a glovebox. The silica jacket was sealed under a 10^{-3} Pa atmosphere and then placed in a temperature-controlled furnace. The sample was heated at 75 K/h to 573 K and then to1123 at 12 K/h, where it dwelled 50 h, and then slowly cooled to 873 at 2 K/h, and finally cooled to 300 K within 10 h. The raw products were washed with distilled water three times to remove the excess flux and the chloride byproducts and then dried with ethanol. After washing, the Rb- and Cs-series products were X-ray pure (Figure 1, Supporting Information S1−S8), but the K-series were mixture of target compounds together with Cu/Te binaries (such as $Cu_{2.86}Te_2$ and Cu_7Te_4) and minor binary $RETe_2$ phase (Supporting Information Figures S9−S12). All the title compounds crystallized as gray blocks or rods and were stable in air at room temperature.

Synthesis of the Pellet for Thermoelectric Property Measurement. The mixture of 20 mmol of CsCl, 24 mmol of RE, 50 mmol of Cu, and 60 mmol of Te (total loading weight is about 18 g) were placed in a silica tube (φ11 × 13 mm). The silica tube was then evacuated, sealed, and placed perpendicularly inside a temperature-controlled furnace. The sample was heated at 75 K/h to 873 K and then at 12 K/h to 1273 K and dwelled for 50 h, and then cooled at 10 K/h to 873 K, at which point the power to the furnace was turned off. Such a process generated an ingot of $Cs_xRE_2Cu_{6-x}Te_6$ inside the silica jacket. A series XRD analyses on the ingot showed that the bottom of the ingot (about 4−5 mm in thickness) was mostly the title compound and minor CsCl impurity, (Figure 2) while the upper part of the ingot was mainly a eutectic mixture of CsCl and Cs_3RECl_6.[17−19] (Supporting Information Figure S17−20) The amount of CsCl had been detected by XRD, EDX, ICP, and chlorine titration as discussed below. The thermal diffusivity and heat capacity were measured on a disk (diameter, ∼11 mm; thickness, ∼4 mm) cut from the bottom part of the ingot, and further polished with sandpaper into a size of ∼10 mm in diameter and ∼3 mm in thickness without washing. The measured density of the pellet was ∼92% of the theoretical density. Subsequently, the disk was cut into a rectangular bar (∼9 × 3 × 2 mm^3) on which the Seebeck coefficient and electrical conductivity were measured. After three runs of the heating and cooling treatment on the pellet during the measurement, the XRD analyses did not show changes in either the phase identity or the percentage of each phase (Figure 2).

Crystal Structure Determinations. The single-crystal XRD data were collected on a Rigaku SCXmini CCD diffractometer equipped with a graphite-monochromated Mo Kα radiation source (λ = 0.71073 Å) at 293 K. The absorption corrections were done by the multiscan method.[20] The space group was determined to be $P6_3/m$ (No. 176) according to the systematic absence, E-value statistics, and subsequent successful refinement of the crystal structure. All structure were solved by the direct method and refined by the full-matrix least-squares fitting on F^2 by SHELX-97.[21] All of the atoms were refined with anisotropic thermal parameters and a secondary extinction correction. As an example, the crystal structure refinement of $Cs_{0.73(2)}Pr_2Cu_{5.27(2)}Te_6$ was discussed in detail. The Cs and Cu sites were first refined with full occupancy, which resulted in a very large atomic displacement parameter of 0.30(4) $Å^2$ for Cs in comparison with those of Pr (0.01 (2) $Å^2$), Cu (0.024(2) $Å^2$), and Te (0.013(2) $Å^2$) and large R values of R_1 = 0.0806 and wR_2 = 0.3678. The refined stoichiometry at this stage was "$Cs_2Pr_2Cu_6Te_6$", which was charge unbalanced if the conventional formal oxidation state was assigned as "$Cs_2^+Pr_2^{3+}Cu_6^+Te_6^{2-}$". Subsequently, the occupancy of Cs and Cu were allowed to vary, and refinement generated occupancies of 35.5(3) and 85.3(3)% at Cs1 and Cu sites and relatively low R values of R_1 = 0.0148 and wR_2 = 0.0302, but a very large atomic displacement parameter of 0.160(3) $Å^2$ on Cs1 site in comparison with those of Pr (0.0143(2) $Å^2$), Cu (0.0188(3) $Å^2$) and Te (0.0161(2) $Å^2$). The Cs1 site also exhibited highly anisotropic displacement parameters with $U_{33} \approx 20U_{11} \approx 20U_{22}$. Such a large atomic displacement parameter usually reflected great disorder. Thus, a weak restraint of ISOR was applied to allow an anisotropic refinement of Cs1 site. However, such a treatment only decreased the U_{eq} from 0.160(3) to 0.126(4) $Å^2$ and generated a large residual peak of 2.63 $Å^2$ around Cs1 site at a distance of 2.498 Å, and the occupancies on Cs1 and Cu sites, as well as the R values were nearly unaffected (35.3(7)%,

dx.doi.org/10.1021/cm201574a |Chem. Mater. 2011, 23, 4910–4919

Table 1. Crystallographic Data for $A_xRE_2Cu_{6-x}Te_6$ (A = K−Cs; RE = La−Nd)[a]

	$Cs_{0.75(2)}La_2Cu_{5.25(2)}Te_6$	$Cs_{0.77(2)}Ce_2Cu_{5.23(2)}Te_6$	$Cs_{0.73(2)}Pr_2Cu_{5.27(2)}Te_6$	$Cs_{0.75(2)}Nd_2Cu_{5.25(2)}Te_6$
fw	1476.69	1480.5	1479.3	1487.34
a (Å)	10.0841(6)	10.0777(7)	10.0763(8)	10.0695(9)
c (Å)	4.2366(6)	4.1918(5)	4.1702(5)	4.1461(8)
V (Å^3)	373.10(6)	368.68(6)	366.68(6)	364.07(8)
D_c (g/cm^3)	6.572	6.668	6.699	6.784
μ (mm^{-1})	26.184	26.897	27.439	28.096
R_1, wR_2 ($I > 2\sigma(I)$) [b]	0.0202,0.0386	0.0203,0.0437	0.0183, 0.0408	0.0235, 0.0443
R_1, wR_2 (all data)	0.0210,0.0389	0.0207,0.0439	0.0189, 0.0412	0.0242, 0.0446
	$Rb_{0.72(2)}La_2Cu_{5.29(2)}Te_6$	$Rb_{0.71(2)}Ce_2Cu_{5.29(2)}Te_6$	$Rb_{0.65(2)}Pr_2Cu_{5.35(2)}Te_6$	$Rb_{0.70(2)}Nd_2Cu_{5.30(2)}Te_6$
fw	1440.45	1442.64	1442.91	1450.68
a (Å)	10.0056(8)	10.0014(8)	9.9955(6)	9.9985(8)
c (Å)	4.2336(6)	4.1976(6)	4.1643(5)	4.1487(6)
V (Å^3)	367.05(7)	363.62(7)	360.31(5)	359.18(7)
D_c (g/cm^3)	6.517	6.588	6.650	6.707
μ (mm^{-1})	27.196	27.818	28.402	29.034
R_1, wR_2 ($I > 2\sigma(I)$) [a]	0.0231, 0.0498	0.0190, 0.0414	0.0208, 0.0456	0.0211, 0.0507
R_1, wR_2 (all data)	0.0240, 0.0503	0.0198, 0.0417	0.0209, 0.0457	0.0212, 0.0507
	$K_{0.73(2)}La_2Cu_{5.27(2)}Te_6$	$K_{0.73(2)}Ce_2Cu_{5.27(2)}Te_6$	$K_{0.76(2)}Pr_2Cu_{5.24(2)}Te_6$	$K_{0.77(2)}Nd_2Cu_{5.23(2)}Te_6$
fw	1407.06	1409.25	1410.09	1416.51
a (Å)	9.955(3)	9.9649(9)	9.9598(7)	9.9683(6)
c (Å)	4.228(3)	4.2042(9)	4.1763(6)	4.1590(5)
V (Å^3)	362.8(3)	361.54(9)	358.78(6)	357.90(5)
D_c (g/cm^3)	6.439	6.473	6.526	6.572
μ (mm^{-1})	25.318	25.785	26.396	26.896
R_1, wR_2 ($I > 2\sigma(I)$) [b]	0.0268, 0.0613	0.0203, 0.0422	0.0200, 0.0438	0.0139, 0.0305
R_1, wR_2 (all data)	0.0274, 0.0617	0.0210, 0.0426	0.0203, 0.0439	0.0147, 0.0308

[a] For all structures, $Z = 1$, space group = $P6_3/m$, $T = 293(2)$ K, and $\lambda = 0.71073$ Å. [b] $R_1 = \Sigma||F_o| - |F_c||/\Sigma|F_o|$, $wR_2 = [\Sigma w(F_o^2 - F_c^2)^2/\Sigma w(F_o^2)^2]^{1/2}$.

85.3(7)%, $R_1 = 0.0172$ and $wR_2 = 0.0388$). Subsequently, this residual peak was assigned as Cs2 and further refinement generated occupancies of Cs1, 23(1)%; Cs2, 13(1)%; Cu, 85.4(5)% and relatively low R values of $R_1 = 0.0161$ and $wR_2 = 0.0354$ with comparable atomic displacement parameters of Cs1, 0.058(4) Å^2; Cs2, 0.054(5) Å^2; Pr, 0.0142(2) Å^2; Cu, 0.0189(4) Å^2; and Te, 0.0160(2) Å^2. Note that the split on Cs sites did not affect the occupancy on Cu site significantly. The refinement at this stage generated a formula of $Cs_{0.72(2)}Pr_2Cu_{5.10(2)}Te_6$, which was close to the neutral "$CsPr_2Cu_5Te_6$" composition. Note that the occupancy of Cu^+ cation should be correlated with that of A^+ according to requirement of charge neutrality, the addition of A^+ cation is to replace the loss of the valence electrons owing to deficiency of Cu^+. So the occupancies of Cs sites (2*a* and 2*b*) and Cu site (6*h*) should sum up to unity. Subsequently, a linear free variable constraint (SUMP) has been applied. Finally, the constrained refinements gave a charge balanced formula of $Cs_{0.73(4)}Pr_2Cu_{5.27(2)}Te_6$. This was supported by the RE/Cu/Te ratio measured by ICP on the same single crystal: $Pr_{1.90}Cu_{5.08}Te_6$. (Supporting Information) All the title compounds had been refined by the similar refinement processes. The single crystal diffraction data showed that as the radii of alkali metal decreased on going from Cs to K, the corresponding atomic displacement parameter increased. For example, before ISOR restraint, K had a U_{eq} = 1.00(2) Å^2 in $K_xPr_2Cu_{6-x}Te_6$ and Rb had a U_{eq} = 0.22(2) Å^2 in $Rb_xPr_2Cu_{6-x}Te_6$. The isostructural title $A_xRE_2Cu_{6-x}Te_6$ compounds (A = K − Cs; RE = La − Nd;) are slightly different in stoichiometries owing to different occupancies on A and Cu sites.

Table 1 summarized the crystallographic data and structural refinement details, the atomic positions, anisotropic displacement parameters, and occupancies were listed in Table 2. And some important bond distances were listed in Table3. Detailed crystallographic data were given in Supporting Information in Table S1. Some important data explaining the refinement process described above were listed in Supporting Information Table S2.

It is worth to mention that the refinement results without SUMP constraint deviate slightly within several percent from those with constraint, nominated as $A_xRE_2Cu_{6y}Te_6$, which may indicate a slight hole-doping in these compounds. For comparison, the corresponding crystallographic data are also provided in Supporting Information, Tables S3 and S4.

Elemental Analyses. Microprobe elemental analyses were performed on several single crystals of the title compounds. Spectra were collected on a field emission scanning electron microscope (FESEM, JSM6700F) equipped with an energy dispersive X-ray spectroscope (EDX, Oxford INCA). Take $Cs_{0.75(2)}La_2Cu_{5.25(2)}Te_6$ for example, the EDX results indicated the presence of Cs, La, Cu, and Te, and no Cl from the flux or Si and O from the silica tube was detected in any case. The EDX analyses gave a stoichiometry of $Cs_{0.9(1)}La_{1.9(2)}Cu_{4.7(2)}Te_6$ (Supporting Information). This is consistent with the single crystal refined composition.

An Ultima-2 inductively coupled plasma emission spectrometer (ICP-OES) was used to quantitatively determine the composition of the title compounds. The measured RE/Cu/Te molar ratios agree well with the single crystal refinement results. For example ICP results of the RE/Cu/Te ratio on La- and Pr-single crystal were $La_{1.92}Cu_{5.03}Te_6$, and $Pr_{1.90}Cu_{5.08}Te_6$. On the other hand, the ICP measured on the bottom

dx.doi.org/10.1021/cm201574a |*Chem. Mater.* 2011, 23, 4910–4919

Table 2. Atomic Coordinates (Å × 10^{-4}), Equivalent Isotropic Displacement Parameters (Å^2 × 10^{-3}), and Site Occupancies for $A_xRE_2Cu_{6-x}Te_6$ (A = K−Cs; RE = La−Nd)

atom	Wyckoff	x	y	z	U(eq)[a]	occu.
		$Cs_{0.75(2)}La_2Cu_{5.25(2)}Te_6$				
Cs1	2a	0	0	2500	58(4)	0.25(1)
Cs2	2b	0	0	0	52(5)	0.13(1)
La	2d	6667	3333	2500	17(1)	1
Cu	6h	5684(1)	6040(1)	2500	22(1)	0.874(2)
Te	6h	2768(1)	3934(1)	2500	17(1)	1
		$Cs_{0.77(2)}Ce_2Cu_{5.23(2)}Te_6$				
Cs1	2a	0	0	2500	55(4)	0.25(1)
Cs2	2b	0	0	0	52(5)	0.14(2)
Ce	2d	6667	3333	2500	14(1)	1
Cu	6h	5675(1)	6023(1)	2500	21(1)	0.872(2)
Te	6h	2756(1)	3949 (1)	2500	16(1)	1
		$Cs_{0.73(2)}Pr_2Cu_{5.27(2)}Te_6$				
Cs1	2a	0	0	2500	57(4)	0.23(1)
Cs2	2b	0	0	0	55(5)	0.14(1)
Pr	2d	6667	3333	2500	14(1)	1
Cu	6h	5666(1)	6005(1)	2500	20(1)	0.878(2)
Te	6h	2742(1)	3955(1)	2500	16(1)	1
		$Cs_{0.75(2)}Nd_2Cu_{5.25(2)}Te_6$				
Cs1	2a	0	0	2500	53(4)	0.23(2)
Cs2	2b	0	0	0	52(5)	0.14(2)
Nd	2d	6667	3333	2500	14(1)	1
Cu	6h	5660(1)	5994(1)	2500	19(1)	0.875(2)
Te	6h	2733(1)	3960(1)	2500	16(1)	1
		$Rb_{0.72(2)}La_2Cu_{5.29(2)}Te_6$				
Rb1	2a	0	0	2500	58(5)	0.20(2)
Rb2	2b	0	0	0	56(6)	0.16(2)
La	2d	6667	3333	2500	16(1)	1
Cu	6h	5672(1)	6026(1)	2500	20(1)	0.881(3)
Te	6h	2741(1)	3893(1)	2500	16(1)	1
		$Rb_{0.71(2)}Ce_2Cu_{5.29(2)}Te_6$				
Rb1	2a	0	0	2500	53(5)	0.19(2)
Rb2	2b	0	0	0	53(5)	0.16(2)
Ce	2d	6667	3333	2500	13(1)	1
Cu	6h	5663(1)	6005(1)	2500	19(1)	0.882(2)
Te	6h	2729(1)	3911(1)	2500	14(1)	1
		$Rb_{0.65(2)}Pr_2Cu_{5.35(2)}Te_6$				
Rb1	2a	0	0	2500	47(5)	0.17(2)
Rb2	2b	0	0	0	57(6)	0.16(2)
Pr	2d	6667	3333	2500	13(1)	1
Cu	6h	5657(1)	5995(1)	2500	19(1)	0.891(3)
Te	6h	2718(1)	3912(1)	2500	15(1)	1
		$Rb_{0.70(2)}Nd_2Cu_{5.30(2)}Te_6$				
Rb1	2a	0	0	2500	49(5)	0.18(2)
Rb2	2b	0	0	0	54(5)	0.17(2)
Nd	2d	6667	3333	2500	13(1)	1
Cu	6h	5655(1)	5986(1)	2500	19(1)	0.884(3)
Te	6h	2713(1)	3927(1)	2500	15(1)	1

Table 2. Continued

atom	Wyckoff	x	y	z	U(eq)[a]	occu.
		$K_{0.73(2)}La_2Cu_{5.27(2)}Te_6$				
K1	2a	0	0	2500	70(8)	0.22(2)
K2	2b	0	0	0	35(8)	0.14(2)
La	2d	6667	3333	2500	17(1)	1
Cu	6h	5665(1)	6014(1)	2500	20(1)	0.879(4)
Te	6h	2724(1)	3872(1)	2500	17(1)	1
		$K_{0.73(2)}Ce_2Cu_{5.27(2)}Te_6$				
K1	2a	0	0	2500	54(8)	0.16(2)
K2	2b	0	0	0	72(8)	0.21(2)
Ce	2d	6667	3333	2500	14(1)	1
Cu	6h	5658(1)	5999(1)	2500	19(1)	0.878(3)
Te	6h	2712(1)	3883(1)	2500	15(1)	1
		$K_{0.76(2)}Pr_2Cu_{5.24(2)}Te_6$				
K1	2a	0	0	2500	42(7)	0.16(2)
K2	2b	0	0	0	69(7)	0.22(2)
Pr	2d	6667	3333	2500	14(1)	1
Cu	6h	5654(1)	5988(1)	2500	18(1)	0.873(3)
Te	6h	2705(1)	3896(1)	2500	15(1)	1
		$K_{0.77(2)}Nd_2Cu_{5.23(2)}Te_6$				
K1	2a	0	0	2500	40(6)	0.16(2)
K2	2b	0	0	0	71(7)	0.22(2)
Nd	2d	6667	3333	2500	10(1)	1
Cu	6h	5650(1)	5978(1)	2500	15(1)	0.872(3)
Te	6h	2698(1)	3902(1)	2500	12(1)	1

[a] U(eq) is defined as one-third of the trace of the orthogonalized U_{ij} tensor.

parts of the corresponding sintered ignots indicated RE/Cu/Te ratios were $La_{2.02}Cu_{5.01}Te_6$, $Ce_{1.93}Cu_{5.01}Te_6$, and $Pr_{1.92}Cu_{5.00}Te_6$, which suggested that the bottom parts did not contain significant impurities. (Supporting Information)

The chloride ion concentration had been measured by titration (Volhard's Method). The bottom part of the sintered ingot (5 mm in thickness) were cut down and ground to fine powders. A 1 g of such fine powders were weighed and dissolved in 50 mL of distilled water and stirred for half an hour. The filtrate had been titrated to determine the chloride concentration according to Volhard's Method. The chloride ion concentration for the bottom part of the ingot of La-, Ce- and Pr-sample is about 3, 3.7, and 5 mmol/L, respectively. Namely, 1 g of samples contain 0.15, 0.185, and 0.25 mmol Cl^-, which are equivalent to 0.025, 0.031, and 0.042 g of CsCl. (Support Information)

Powder XRD. The powder XRD patterns were taken at room temperature on a RigakuDMAX2500 powder diffractometer or Rigaku MiniFlex II powder diffractometer with monochromatized Cu Kαradiation. Data were collected at a scanning rate of 5°/min over 2θ ranging from 5° to 70° or 85°.

Magnetic Susceptibility Measurements. The dc magnetic susceptibility measurements were performed on a Quantum Design MPMS-XL magnetometer for the $Cs_xRE_2Cu_{6-x}Te_6$ (RE = Ce, Pr, Nd) in the temperature range of 2−300 K. The X-ray pure polycrystalline samples were ground to fine powders to minimize the possible anisotropic effects and loaded into a gelatin capsule. The data were corrected for the susceptibility of the container and for the diamagnetic contribution from the ion core.

Electronic Structure Calculations. The dentity functional calculations were performed using the Vienna ab initio simulation package

dx.doi.org/10.1021/cm201574a |Chem. Mater. 2011, 23, 4910–4919

Table 3. Selected Bonds Distances (Å) for $A_xRE_2Cu_{6-x}Te_6$ (A = K−Cs; RE = La−Nd)

	Cs−La	Cs−Ce	Cs−Pr	Cs−Nd	Rb−La	Rb−Ce
A1−Te × 3	3.530(1)	3.536(1)	3.536(1)	3.536(1)	3.466(1)	3.474(1)
A1−Te × 3	4.116(1)	4.110(1)	4.105(1)	4.099(1)	4.061(1)	4.059(1)
A2−Te × 6	3.685(1)	3.688(1)	3.686(1)	3.684(1)	3.624(1)	3.629(1)
RE−Te × 6	3.291(1)	3.262(1)	3.247(1)	3.232(1)	3.300(1)	3.271(1)
Cu−Te × 2	2.624(1)	2.617(1)	2.619(1)	2.616(1)	2.623(1)	2.618(2)
Cu−Te × 1	2.629(2)	2.621(2)	2.620(2)	2.617(2)	2.626(2)	2.620(1)
Cu−Te × 1	2.645(2)	2.636(2)	2.633(2)	2.628(2)	2.634(2)	2.626(2)
Cu−Cu × 2	2.810(2)	2.773(2)	2.745(2)	2.723(2)	2.782(2)	2.746(2)
	Rb−Pr	Rb−Nd	K−La	K−Ce	K−Pr	K−Nd
A1−Te × 3	3.471(1)	3.482(1)	3.429(2)	3.438(1)	3.444(1)	3.450(1)
A1−Te × 3	4.047(1)	4.053(1)	4.028(2)	4.030(1)	4.028(1)	4.028(1)
A2−Te × 6	3.624(1)	3.633(1)	3.588(1)	3.595(1)	3.599(1)	3.603(1)
RE−Te × 6	3.256(1)	3.239(1)	3.300(2)	3.283(1)	3.262(1)	3.252(1)
Cu−Te × 2	2.614(1)	2.614(1)	2.621(2)	2.622(1)	2.615(1)	2.615(1)
Cu−Te × 1	2.617(2)	2.614(1)	2.622(2)	2.622(1)	2.617(1)	2.617(1)
Cu−Te × 1	2.621(2)	2.615(2)	2.625(2)	2.623(1)	2.619(1)	2.618(1)
Cu−Cu × 2	2.722(2)	2.707(2)	2.762(2)	2.737(2)	2.714(2)	2.700(1)

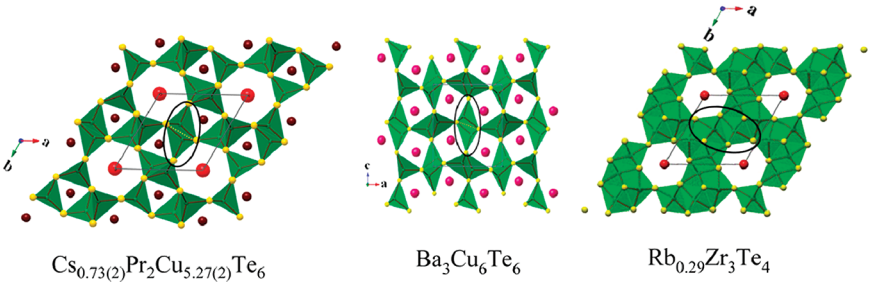

Figure 3. Crystal structures of (left) $Cs_{0.73(2)}Pr_2Cu_{5.27(2)}Te_6$ view along [001]. (middle) $Ba_3Cu_6Te_6$ view along [010].[14] (left) $Rb_{0.29}Zr_3Te_4$ view along [001].[26] Green: Cu or Zr. Yellow: Te. Red: A. Dark red: Pr. Red: Ba. The circle indicates the $CuTe_4$ double-tetrahedron-chain or $ZrTe_6$ octahedron-based-chain.

VASP[22] with plane waves as basis set. The geometry optimization and band structure calculations were performed within the projector augmented wave (PAW)[23] method and the generalized gradient approximation (GGA)[24] expressed by Perdew-Burke-Ernzerhof (PBE)[25] functional. A Gamma centered Monkhorst-Pack k-point mesh of 3 × 3 × 8 and 12 × 12 × 32 were chosen for Brillouin-zone integration in the self-convergence calculation and for density of states (DOS) calculations, respectively.

Since the presence of the partial occupancy, a hypothetical compound was therefore built according to the crystallographic structure as followed. One of the six Cu atoms at *6h* site was eliminated and only one Cs atom at (0, 0, 0.25) was remained in the unit cell, thus the space group was reduced to *P*1, and a formula of "$CsLa_2Cu_5Te_6$" is generated, which is in fact the ideal composition (charge balanced formulas) of the title compounds.

Thermoelectric Property Measurements. The thermal diffusivity and heat capacity of $Cs_xRE_2Cu_{6-x}Te_6$ were measured by laser flash techniques with a Netzsch LFA 457 system in an Ar atmosphere with pyroceram 9606 as the standard for heat capacity measurement. The thermal conductivity was calculated according to the equation $\kappa(T) = \alpha(T)Cp(T)\rho(T)$, in which $\rho(T)$ is the experimental density, Cp (T) the heat capacity, and $\alpha(T)$ the measured thermal diffusivity. The Seebeck coefficient and electrical conductivity were measured on a ULVAC ZEM-3 instrument from room temperature to about 700 K. Each curve was measured three times in the temperature range to ensure the stability and repeatability of the data.

RESULTS AND DISCUSSION

Syntheses. Pure-phased Cs-, Rb-compounds can be synthesized. (Figure 1, Supporting Information S1−8) Considering the charge balanced formula $ARE_2Cu_5Te_6$ of title compounds, the reactions may be expressed by eq 1 as followed. In powdery samples, the byproducts A_3RECl_6 and ACl will react with water[18] and thus can be washed out (Supporting Information Figures S17 and S18) But the hot-press technique cannot make a dense pellet from such pure powders (suffering with low density, spallation). Thus, a direct sintering route on large scale with a total loading weight of about 18 g has to develop to produce a highly compact ingot. As discussed above, the bottom part of the ingot is the title compound together with enwrapped minor CsCl impurity (2 − 4%). The drawback of such a route is that CsCl imbedded inside the ingot cannot be washed out by immergence without grinding. All in all, such a direct sintering method is the best approach at present to produce pellets

dx.doi.org/10.1021/cm201574a |*Chem. Mater.* 2011, 23, 4910–4919

exhibiting properties that are the closest to the intrinsic TE properties of the title compounds.

$$2.4RE + 5Cu + 6Te + 3ACl(excess) \xrightarrow{1123\ K} ARE_2Cu_5Te_6 + 0.4A_3RECl_6 + 0.8ACl \quad (1)$$

Crystal Structures. The title compounds are isostructural compounds with slightly different stoichiometries owing to different occupancies on A and Cu sites. (Table 2) These compounds feature a novel 3D anionic $CuTe_4$-based framework that embeds two kinds of tunnels along the *c* axis, larger hexagonal ones accommodating larger A^+ cations and smaller trigonal tunnels accommodating smaller RE^{3+} cations (Figure 3). Cu atom is coordinated in a slightly distorted $CuTe_4$ tetrahedron. Each $CuTe_4$ tetrahedron shares two neighboring edges with two other $CuTe_4$ tetrahedra forming a double-tetrahedron-chain extending along *c* axis as indicated by a circle in Figure 3 left. Three such double-tetrahedron-chains (Figure 4) are connected by sharing the tetrahedron apexes to confine a trigonal tunnel that accommodates RE^{3+} cations (Figure 3). Meanwhile, six double-tetrahedron-chains are arranged in a manner that a hexagonal tunnel containing larger A^+ cations is confined (Figure 3). Another way to describe such a structure is that a hexagonal tunnel is surrounded by six small trigonal tunnels (Figure 3).

The Cu/Te framework of $A_xRE_2Cu_{6-x}Te_6$ is a resemblance of that of $Ba_3Cu_6Te_6$.[14] (Figure 3) A simple comparison suggests a substitution of 3 Ba^{2+} with a combination of *x* A^+ and 2 RE^{3+} on going from $Ba_3Cu_6Te_6$ to $A_xRE_2Cu_{6-x}Te_6$. Such a substitution donates about one more electron to the Cu/Te framework; therefore, the charge neutrality requires a deficiency on Cu site, which has been seen in the single crystal refinement results. Thus the charge balanced formulas can be noted as "$(A^+)_x(RE^{3+})_2(Cu^+)_{6-x}(Te^{2-})_6$" vs "$(Ba^{2+})_3(Cu^+)_6(Te^{2-})_6$". The VASP calculations, as well as the diamagnetic property of $Cs_{0.75(2)}La_2Cu_{5.25(2)}Te_6$ discussed below, also suggest that the formal oxidation state of Cu is +1. Such a cationic substitution seems to result in an anionic structural reconstruction in order to accommodate different cations, RE^{3+} and A^+, from a single-rhombic tunnel-structure in $Ba_3Cu_6Te_6$[14] (Figure 3) to a double-tunnel-structure (Figure 3). Besides, the framework of title compounds are totally different from those in some related compounds, such as $A_3RE_4Cu_5Te_{10}$,[6,7] $CsRE_2CuTe_4$,[8,9] and $CsSc_3Cu_2Te_6$,[9] in which the $CuTe_4$-tetrahedron-chains together with $RETe_6$ octahedra define the tunnels accommodating merely alkali metal atoms. Yet, the title compounds and $A_xZr_3Te_4$[26] (Figure 3) share common space group, Wyckoff site set, and similar unit cell dimensions; both feature large hexagonal tunnels that are partially centered by the alkali metals. Interestingly, $Rb_{0.29}Zr_3Te_4$ also shows a similar site split for alkali metal over 2*a* and 2*b* sites.[26] The major structure difference lies in the different anionic 3D frameworks, $CuTe_4$ tetrahedron-based framework vs $ZrTe_6$ octahedron-based framework, which is caused by the different atom identities on three sites: La vs Te on 2*d* site; Cu vs Te on 6*h*; and Te vs Zr on another 6*h* site[26] (Figure 3).

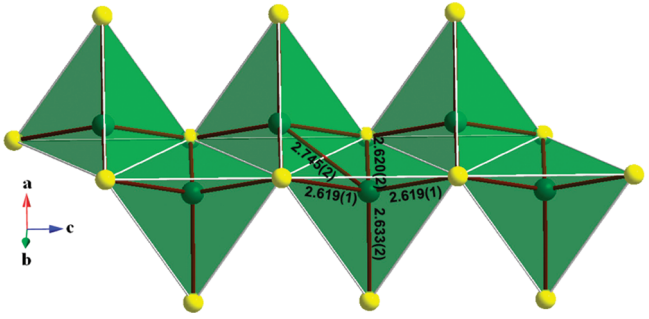

Figure 4. $CuTe_4$ double-tetrahedron-chain extending along *c* direction in $Cs_{0.73(2)}Pr_2Cu_{5.27(2)}Te_6$. Green: Cu, yellow: Te. The Cu−Te distances (Å) are marked.

Figure 4 shows $CuTe_4$ tetrahedron propagates down *c* axis as a double-tetrahedron-chain via sharing two neighboring edges. The similar double-chain has also been found in $CsSc_3Cu_2Te_6$.[9] As listed in Table 1, the average occupancy on Cu site is of 0.86(1). The fractional occupancy on Cu site is also found in other copper tellurides, such as $Cu_{2-x}Te$,[27a] $TlCu_{2-x}Te_2$[27b] and $Ba_3Cu_{14-x}Te_{12}$.[10] As shown in Figure 3, the $CuTe_4$ tetrahedron also shares all apexes with neighboring chains. The Cu−Te distances of 2.614(1)−2.645(2) Å are consistent with those of 2.591(2)−2.820(2) Å in $Rb_2CeCu_3Te_5$[4] and 2.599(2) − 2.784(5) Å in $Ba_3Cu_6Te_6$.[14] The Cu−Cu distances, 2.700(1) − 2.810(2) Å, are comparable to those of $Rb_2CeCu_3Te_5$ (2.650(2) Å)[4] and $Ba_3Cu_6Te_6$ (2.847(5) Å).[14]

The coordination environments of RE^{3+} are trigonal prisms with six RE−Te distances varying in the range of 3.232(1)−3.300(2) Å. These distances are consistent with the previously reported distances of 3.175(1)−3.254(1) Å in $CsRECdTe_3$[28] and $Rb_2CeCu_3Te_5$.[4] The $PrTe_6$ trigonal prisms form infinite $[PrTe_3]$ chains by face-sharing along the [001] direction. (Figure 3) The RE−Te distances show typical lanthanide contraction and monotonic shrinking with the increase of 4f electrons of the RE^{3+} ion. (Table 3) As a result, the *c* axis that is

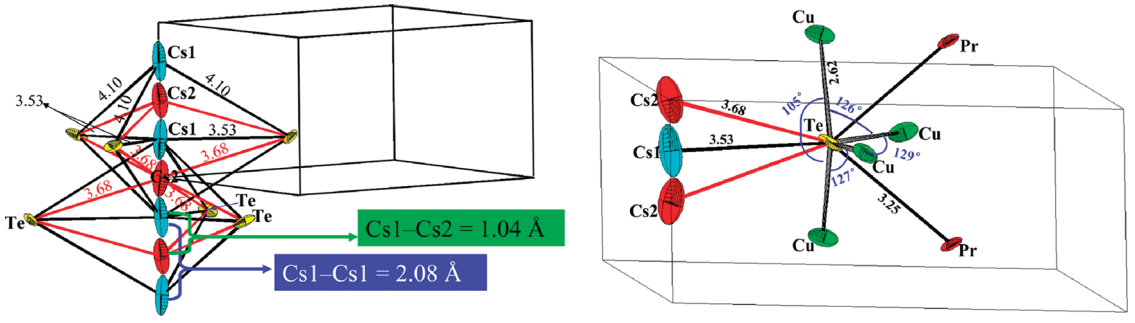

Figure 5. (left) The anisotropic thermal elipsoids of Cs atoms disorder over 2*a* (0, 0, 0.25) and 2*b* (0, 0, 0) sites. The Cs−Te and Cs−Cs distances (Å) are marked. (right) The anisotropic behavior of Te atom with distances (Å) and angles marked.

dx.doi.org/10.1021/cm201574a |*Chem. Mater.* 2011, 23, 4910–4919

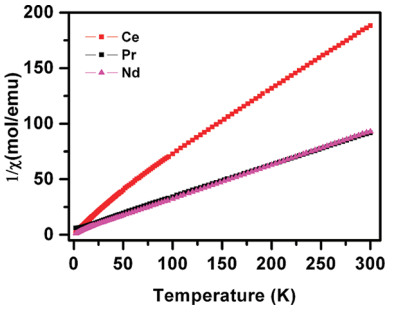

Figure 6. Plots of $1/\chi_M$ vs temperature for $Cs_xRE_2Cu_{6-x}Te_6$ (RE = Ce, Pr, Nd).

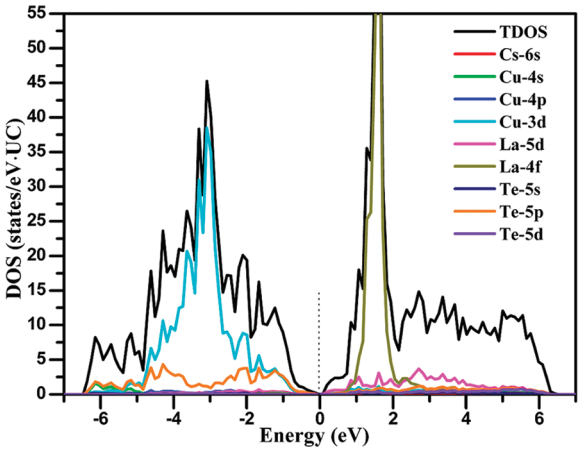

Figure 7. Total and partial DOS of hypothetical $CsLa_2Cu_5Te_6$.

parallel to the infinite $[PrTe_3]$ chains is mostly affected by the RE−Te distances and consequently shortens with the increase of the atomic number of RE. (Table 1) Meanwhile, the *a* axis is affected by not only RE−Te distances but also occupancies of A^+ and Cu^+ cations, as well as the size of A^+, therefore, the *a* axis does not show obvious change on the identity of the RE atom (Table 1).

The A−Te bond distances exhibit a larger range: Cs−Te, 3.530(1)−4.116(1) Å; Rb−Te, 3.466(1)−4.061(1) Å; and K−Te, 3.429(2)−4.030(1) Å, which are comparable to those in other compounds, such as $Cs_2Cd_3Te_4$ [3.883(1)−4.003(1) Å],[29] CsRECdTe$_3$ [3.810(5)−4.201(2) Å],[28] $Rb_3Cu_8Te_{10}$ [3.698(6)−4.190(9) Å],[11] $K_4Zr_3Te_{17}$ [3.457(1)−4.092(1) Å],[30] and $K_4Cu_8Te_{11}$ [3.676(3) − 3.960(3) Å].[11] Since the disorder, the local coordination spheres around Cs atoms are of great distortion. (Figure 5) The size of A atom is diminished from Cs to K, as a result, the *a* axis is shortened on going from Cs to K (Table 1, from top to bottom). However, the *c* axis, which is parallel to the extending direction of the tunnels filled by A, is nearly not influenced. We considered this is related to the existence of the vacancy of A^+ cations. Also the anisotropic behavior of the Te atom is shown in Figure 5 right, which does not react intensively to the missing of copper atoms.

Magnetic Properties. The magnetic susceptibilities of the $Cs_xRE_2Cu_{6-x}Te_6$ (RE = Ce, Pr, Nd;) were measured over the range 2 − 300K at 1000 Oe, and the plots of the reciprocal of the molar susceptibility ($1/\chi_M$) vs *T* are displayed in Figure 6. The susceptibility data were fit by the least-squares method to the

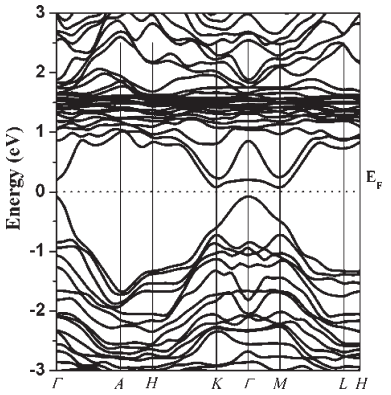

Figure 8. Band structures of hypothetical $CsLa_2Cu_5Te_6$.

Curie−Weiss equation $\chi_M = C/(T - \theta)$, where χ_M is the magnetic susceptibility, *C* is the Curie constant, and θ is the Weiss constant. The effective magnetic moment ($\mu_{eff(total)}$) was calculated from the equation $\mu_{eff(total)} = (7.997C)^{1/2}\mu_B$.[31] The Pr- and Nd-compound obey Curie−Weiss law in the entire experimental temperature region, while the Ce-member deviates from the Curie−Weiss behavior below 50 K. Such a deviation has been reported for several other Ce^{3+} compounds and has been attributed to crystal field splitting of the $^2F_{5/2}$ ground state.[32] For Pr- and Nd-compound, the linear fitting of $1/\chi_M$ with *T* over the whole temperature generated *C*: 3.25 and 3.28 cm^3 mol^{-1} K; θ: −16.40 and −6.32 K; and $\mu_{eff(total)}$: 5.06 and 5.12 μ_B, respectively. For Ce-compound, these values are 1.74 cm^3 mol^{-1} K, −28.42 K and 3.73 μ_B, respectively, at temperatures above 100 K. Since there were 2 RE^{3+} ions per formula, the μ_{eff} values were estimated to be of 2.64 μ_B per Ce^{3+}, 3.58 μ_B per Pr^{3+} and 3.62 μ_B per Nd^{3+} according to the equation $\mu_{eff} = \mu_{eff(total)}/(2^{1/2})$,[33] which are in accordance with the corresponding theoretical values of the isolated magnetic center per formula unit (2.54, 3.58, and 3.62 μ_B, respectively).[34] The negative Weiss constants for all of these compounds indicate a small degree of local antiferromagnetic interaction.

The $4f^0$ nature of La^{3+} and the $3d^{10}$ nature of Cu^+ in $Cs_xLa_2Cu_{6-x}Te_6$ suggest the diamagnetic property of this compound. (Supporting Information Figure S14)

Electronic Structures. To understand the distribution of orbitals in the vicinity of the Fermi level (E_F), the total and partial DOSs were studied based on the non spin-polarized calculations on two hypothetical compounds: "$CsLa_2Cu_5Te_6$" and "$CsPr_2Cu_5Te_6$". Hypothetical $CsLa_2Cu_5Te_6$ shows a small band gap of 0.09 eV (Figure 7), whereas hypothetical $CsPr_2Cu_5Te_6$ shows a pseudo gap (Supporting Information Figure S13). The valence band (VB) of hypothetical $CsLa_2Cu_5Te_6$ is composed of Cu 3d and Te 5p with minor contributions from Cu 4s, Cu 4p, La 5d, and Te 5d; whereas the conduction band (VB) is dominated by La 4f mixed with La 5d, Te 5d and Te 5p. Note that the partial DOS of Cs atom is almost zero at the top of VB as well as near the bottom of CB, which proves that Cs atom acts primarily as an electron donor. The 3d bands of Cu atom locate down below the E_F, and minor 4s and 4p bands have been seen in VB, so copper atom is expected to loss one electron and thus possesses a formal oxidation state of +1, which is confirmed by the diamagnetic property of $Cs_xLa_2Cu_{6-x}Te_6$ (Supporting Information Figure S14).

The band structure of hypothetical $CsLa_2Cu_5Te_6$ shows the VB maximum at Γ point and the CB minimum at *M* point,

dx.doi.org/10.1021/cm201574a |*Chem. Mater.* 2011, 23, 4910–4919

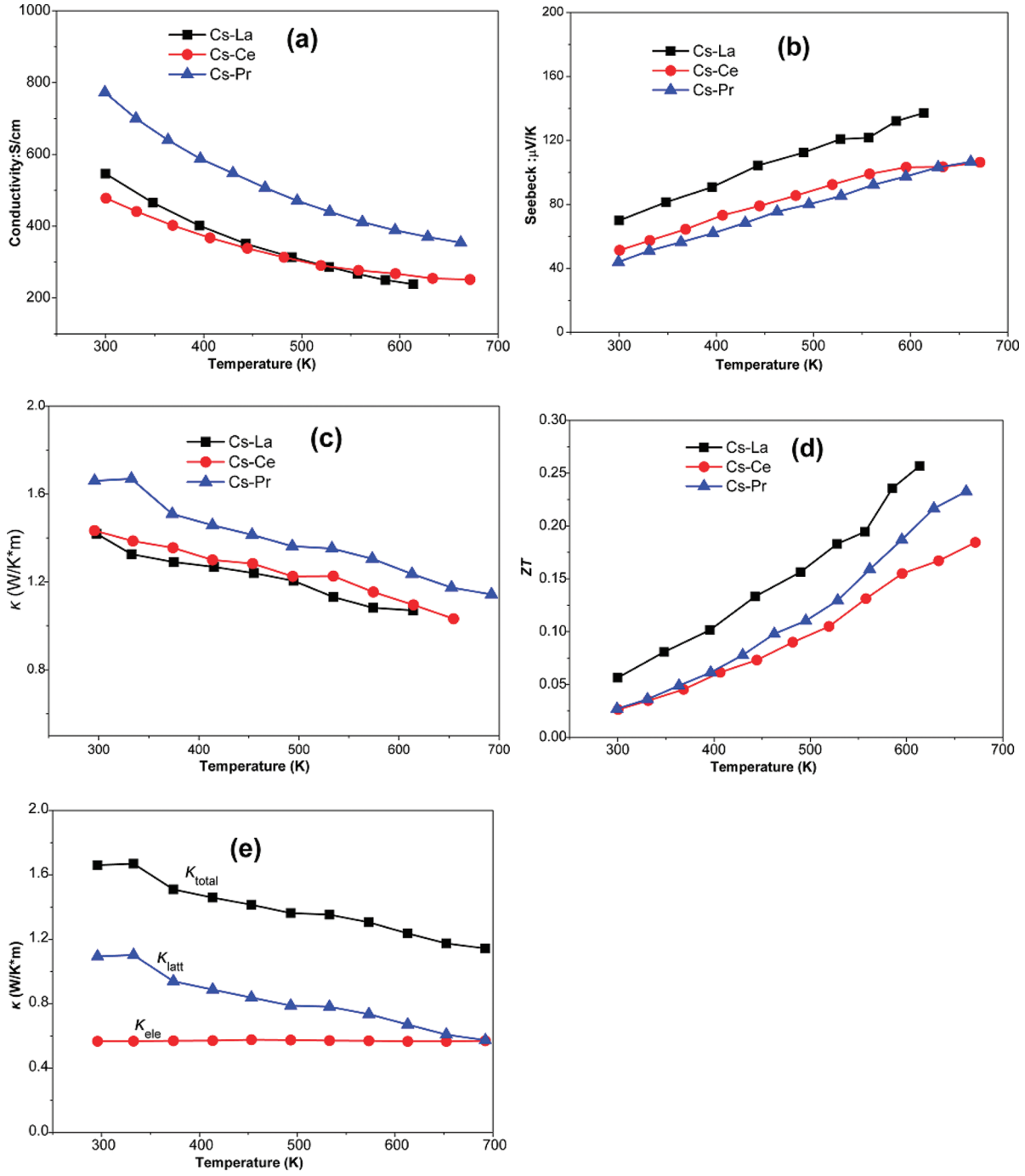

Figure 9. Temperature dependences of (a) electrical conductivity, (b) Seebeck coefficient, (c) total thermal conductivity, (d) ZT, for undoped sintered polycrystalline $Cs_xRE_2Cu_{6-x}Te_6$ pellets (weight percentage of CsCl impurity is 2.5, 3.1, and 4.2% for La-, Ce-, and Pr-sample, respectively); and (e) total thermal conductivity (κ_{total}), lattice thermal conductivity (κ_{latt}) and electric thermal conductivity (κ_{el}) for the $Cs_{0.73(4)}Pr_2Cu_{5.27(2)}Te_6$ pellet. (with 4.2% CsCl impurity).

indicating an indirect narrow gap semiconductor feature (Figure 8). Two CB minima are found at K and M and one VB maximum at Γ, which may be indicative of a high ZT with the electron doping because the number of band minima is proportionally related to the carrier effective mass and thus contribute to the Seebeck coefficient.[35−37] Detailed theoretical studies on thermoelectric property are ongoing, and will be published in a separate article soon.

Electrical and Thermal Transport Properties. As discussed in Syntheses section, small amount of CsCl impurity (2 −4%) exists in the pellets, which will have an effect on the TE properties. However, to remove the CsCl impurity or to quantificationally evaluate the influence of such an impurity is impossible under the current experimental condition. Since the amount of the impurity is not significant, we consider the influence should not be remarkable. Figure 9a shows the metal-like behavior of the

dx.doi.org/10.1021/cm201574a |*Chem. Mater.* 2011, 23, 4910–4919

Table 4. Thermoelectric Property Comparison of Some Selected Undoped Samples

structure type	compound	σ (S/cm)	S (μV/K)	κ_{total} (W/m·K)	κ_{latt} (W/m·K)	ZT	T (K)	ref
tunnel	$Ba_2Cu_6Te_6$[a]	127	+88	2.2	N/A	0.01	295	14
	$Cs_{0.75(2)}La_2Cu_{5.25(2)}Te_6$[a]	546	+70	1.42	1.02	0.05	300	present work
		238	+137	1.07	0.71	0.26	614	
	$Cs_{0.77(2)}Ce_2Cu_{5.23(2)}Te_6$[a]	477	+51	1.43	1.08	0.02	300	present work
		250	+104	1.04	0.60	0.17	660	
	$Cs_{0.73(2)}Pr_2Cu_{5.27(2)}Te_6$[a]	773	+44	1.66	1.09	0.02	300	present work
		354	+106	1.14	0.57	0.23	660	
type-I clathrate	$Ba_8Ga_{16}Ge_{30}$[b]	1562	−45	1.8	0.66	0.05	300	16c
		800	−100	1.63	0.23	0.34	700	
		600	−145	1.66	0.24	0.80	1050	
skutterudite	$CoSb_3$[c]	529	+220	10.2	9.7	0.07	300	16d
layered	$CsBi_4Te_6$[b] (p-type)	900−450	+90−+150	1.21−1.53	~0.87	0.18−0.2	300	16e
NaCl	PbTe (p-type)[a]	256	+265.5	3.18	2.5	0.17	300	16a
layered	Bi_2Te_3 (p-type)[b]	556	+220	1.7	~1	0.27	300	16b
alloy	SiGe (p-type)[a]	877	+121	N/A		N/A	300	16b
		757	+144	4.8		0.13	400	
		518	+189	4.41		0.29	700	
		315	+235	4.45		0.50	1200	

[a] As-synthesized sintered polycrystalline pellet (weight percentage of CsCl impurity is 2.5, 3.1, and 4.2% for La-, Ce-, and Pr-sample, respectively). [b] Single crystal. [c] Cold pressed pellet.

temperature dependence of electrical conductivity for the undoped sintered polycrystalline pellets of $Cs_xRE_2Cu_{6-x}Te_6$. In comparison with that of the single-tunnel structure ternary compound $Ba_3Cu_6Te_6$,[14] these conductivity values are high. (Table 4) Such high electrical conductivities may be attributed to the smaller band gap (calculated $CsLa_2Cu_5Te_6$, 0.09 eV vs $Ba_3Cu_6Te_6$ 0.6 eV[38]). This behavior may also result from the CsCl impurity or defects that produce higher carrier density.[14,27a,38] The positive S for $Cs_xRE_2Cu_{6-x}Te_6$ indicates that the main charge carriers are holes. The Seebeck coefficient increases nearly linearly with increasing temperature as shown in Figure 9b, and reaches 137 μV/K at 614 K, 104 and 106 μV/K at 660 K, for La-, Ce-, and Pr-sample, respectively. The room temperature values are comparable to those of some well-known TE materials, such as skutterudite $CoSb_3$,[16d] type-I clathrate $Ba_8Ga_{16}Ge_{30}$ (n type),[16c] undoped samples of $CsBi_4Te_6$,[16e] and undoped samples of PbTe,[16a] Bi_2Te_3,[16b] and SiGe[16b] (Table 4).

Figure 9c displays the temperature dependence of thermal conductivity. At room temperature, the measured C_p (La, 0.277 J/g·K; Ce, 0.294 J/g·K; Pr, 0.272 J/g·K) is in accordance with the Dulong Petit value (0.236 J/g·K). The temperature dependences of specific heat and thermal diffusivity are given in Supporting Information Figures S15 and S16. The total thermal conductivity (κ_{total}) is low with respect to those listed in Table 4. The lattice thermal conductivity (κ_{latt}) has been estimated by subtracting the electronic thermal conductivity (κ_{ele}) from κ_{total}, according to the Wiedemann−Franz law $\kappa_{ele} = L\sigma T$, where the Lorentz number (L) = 2.45×10^{-8} W·Ω/K^2,[16e,39] The values of the derived κ_{latt} are also comparable to those of $Ba_8Ga_{16}Ge_{30}$, $CsBi_4Te_6$, and Bi_2Te_3 listed in Table 4, which may suggest that the structure of $A_xRE_2Cu_{6-x}Te_6$ can scatter the phonon effectively. This is likely a consequence of the larger thermal displacement parameters of Cs atoms and the deficiency of Cu atoms.[15,40] The larger thermal displacement parameters of Cs atoms suggest that Cs atoms may play a role of rattlers.[41]

The temperature dependence of ZT is calculated and presented in Figure 9d. The ZT value increases with temperature and reaches 0.26 at 614 K, 0.17 and 0.23 at 660 K, for undoped La-, Ce- and Pr-sample, respectively. The band structure feature discussed above indicate that further improvement is possible via the optimization of the composition and doping to change the effective mass, mobility, and the concentration of carriers around E_F.[16e] Furthermore, we found the title compounds are robust and good mechanical property. These primary data distinguish the title compounds as a new promising family of TE material candidate. Further work is ongoing.

CONCLUSION

Novel hexagonal double-tunnel compounds $A_xRE_2Cu_{6-x}Te_6$ (A = K − Cs; RE = La − Nd) have been synthesized from the elemental mixtures in the ACl flux at 1123 K. The $CuTe_4$ tetrahedron-based 3D framework contains both large hexagonal and small trigonal tunnels that accommodate large A^+ or small RE^{3+} cation. The c axes are mostly affected by the RE−Te distances and consequently shorten with the increase of the atomic number of RE owing to the typical lanthanide contraction. The diamagnetic $Cs_xLa_2Cu_{6-x}Te_6$ indicates the +1 formal oxidation state of Cu. The paramagnetic properties of Pr-, Nd- and Ce-members are obeying the Curie−Weiss law. The undoped sintered polycrystalline pellets (containing 2 − 4% CsCl impurity) show relatively high electrical conductivity, moderate Seebeck coefficient and relatively low thermal conductivity and obtain ZTs of 0.26 at 614 K, 0.17 and 0.23 at 660 K, respectively. Both the conductivity and Seebeck coefficient follow a typical behavior of a narrow gap semiconductor or a semi metal as revealed by the VASP calculations. The band structure shows multiple conduction band minima, which may be indicative of a higher ZT via composition optimization and doping. These novel quaternary double-tunnel compounds may represent a new promising family of TE material candidate and further enhancement of the ZT value is possible.

■ ASSOCIATED CONTENT

Supporting Information. The cif data, additional tables containing crystallographic data, unconstrained refinements, and figures of XRD patterns, DOS and band structures. This material is available free of charge via the Internet at http://pubs.acs.org.

■ AUTHOR INFORMATION

Corresponding Author
*E-mail: chenl@fjirsm.ac.cn. Tel: (011)86-591-83704947.

■ ACKNOWLEDGMENT

This research was supported by the National Natural Science Foundation of China under Projects (90922021, 21171168, 20733003, 20973175), the "Knowledge Innovation Program of the Chinese Academy of Sciences" (KJCX2-YW-H20, CXJJ-11-M71).

■ REFERENCES

(1) Mitchell, K.; Ibers, J. A. *Chem. Rev.* **2002**, *102*, 1929–1952.
(2) Patschke, R.; Heising, J.; Kanatzidis, M.; Brazis, P.; Kannewurf, C. R. *Chem. Mater.* **1998**, *10*, 695–697.
(3) Malliakas, C. D.; Kanatzidis, M. G. *J. Am. Chem. Soc.* **2007**, *129*, 10675–10677.
(4) Patschke, R.; Brazis, P.; Kannewurf, C. R.; Kanatzidis, M. G. *J. Mater. Chem.* **1998**, *8*, 2587–2589.
(5) Patschke, R.; Brazis, P.; Kannewurf, C. R.; Kanatzidis, M. G. *J. Mater. Chem.* **1999**, *9*, 2293–2296.
(6) Huang, F. Q.; Choe, W.; Lee, S.; Chu, J. S. *Chem. Mater.* **1998**, *10*, 1320–1326.
(7) Huang, F. Q.; Ibers, J. A. *J. Solid State Chem.* **2001**, *160*, 409–414.
(8) Babo, J. M.; Strobel, S.; Schleid, T. *Z. Anorg. Allg. Chem.* **2010**, *636*, 349–355.
(9) Babo, J. M.; Schleid, T. *Solid State Sci.* **2010**, *12*, 238–245.
(10) Assoud, A.; Thomas, S.; Sutherland, B.; Zhang, H. Q.; Tritt, T. M.; Kleinke, H. *Chem. Mater.* **2006**, *18*, 3866–3872.
(11) Zhang, X.; Park, Y. B.; Hogan, T.; Schindler, J. L.; Kannewurf, C. R.; Seong, S.; Albright, T.; Kanatzidis, M. G. *J. Am. Chem. Soc.* **1995**, *117*, 10300–10310.
(12) Klepp, K. O. *Z Naturforsch. B.* **1987**, *42*, 130–134.
(13) Savelsberg, G.; Schafer, H. *Mater. Res. Bull.* **1981**, *16*, 1291–1297.
(14) Wang, Y. C.; DiSalvo, F. J. *J. Solid State Chem.* **2001**, *156*, 44–50.
(15) *CRC Handbook of Thermoelectrics*; Rowe, D. M., Ed.; CRC Press: Boca Raton, FL, 1995; pp 19−25.
(16) (a) Heremans, J. P.; Thrush, C. M.; Morelli, D. T. *J. Appl. Phys.* **2005**, *98*, 063703–1−6. (b) *CRC Handbook of Thermoelectrics*; Rowe, D. M., Ed.; CRC Press: Boca Raton, FL, 1995; pp 211−236, 329−336. (c) Toberer, E. S.; Christensen, M.; Iversen, B. B.; Snyder, G. J. *Phys. Rev. B* **2008**, *77*, 075203–1−8. (d) Caillat, T.; Borshchevsky, A.; Fleurial, J. P. *J. Appl. Phys.* **1996**, *80*, 4442–4449. (e) Chung, D. Y.; Hogan, T. P.; Rocci-Lane, M.; Brazis, P.; Ireland, J. R.; Kannewurf, C. R.; Bastea, M.; Uher, C.; Kanatzidis, M. G. *J. Am. Chem. Soc.* **2004**, *126*, 6414–6428.
(17) Seifert, H. J. *J. Therm. Anal. Calorim.* **2002**, *67*, 789–826.
(18) (a) Reuter, G.; Frenzen, G. *J. Solid State Chem.* **1995**, *116*, 329–334. (b) Seifert, H. J.; Fink, H.; Baumgartner, B. *J. Solid State Chem.* **1993**, *107*, 19–26.
(19) Seifert, H. J.; Sandrock, J.; Uebach, J. *Z. Anorg. Allg. Chem.* **1987**, *555*, 143–153.
(20) *CrystalClear*, version 1.3.5; Rigaku Corp.: The Woodlands, TX, 1999.
(21) Sheldrick, G. M. *SHELXTL*, version 5.1; Bruker-AXS: Madison, WI, 1998.
(22) Kresse, G.; Furthmuller, J. *Phys. Rev. B* **1996**, *54*, 11169–11186.
(23) Blochl, P. E. *Phys. Rev. B* **1994**, *50*, 17953–17979.
(24) Kresse, G.; Joubert, D. *Phys. Rev. B* **1999**, *59*, 1758–1775.
(25) Perdew, J. P.; Burke, K.; Ernzerhof, M. *Phys. Rev. Lett.* **1996**, *77*, 3865–3868.
(26) Wang, C.; Abdon, R. L.; Hughbanks, T.; Reibenspies, J. *J. Alloys Compd.* **1995**, *226*, 10–18.
(27) (a) Mansour, B. A.; Farag, B. S.; Khodier, S. A. *Thin Solid Films* **1994**, *247*, 112–119. (b) Ohtani, T.; Taniguchi, M.; Sasaki, S.; Kishi, H.; Nakata, T. *J. Alloys Compd.* **2004**, *383*, 245–250.
(28) Liu, Y.; Chen, L.; Wu, L. M. *Inorg. Chem.* **2008**, *47*, 855–862.
(29) Narducci, A. A.; Ibers, J. A. *J. Alloys Compd.* **2000**, *306*, 170–174.
(30) Keane, P. M.; Ibers, J. A. *Inorg. Chem.* **1991**, *30*, 1327–1329.
(31) O'Connor, C. *J. Prog. Inorg. Chem.* **1982**, *29*, 203–283.
(32) Greenwood, N. N.; Earnshaw, A. *Chemistry of the Elements*; Pergamon Press: New York, 1984; p 1443.
(33) West, A. R. *Solid State Chemistry and Its Applications*; John Wiley &Sons: Chichester, U.K., 1984.
(34) Van Vleck, J. H. *The Theory of Electric and Magnetic Susceptibilities*; Oxford University: Oxford, U.K., 1932; pp 226−261.
(35) Hicks, L. D.; Dresselhaus, M. S. *Phys. Rev. B* **1993**, *47*, 12727–12731.
(36) Larson, P.; Mahanti, S. D.; Chung, D. Y.; Kanatzidis, M. G. *Phys. Rev. B* **2002**, *65*, 045205–1−5.
(37) Larson, P.; Mahanti, S. D.; Kanatzidis, M. G. *Phys. Rev. B* **2000**, *61*, 8162–8171.
(38) Assoud, A.; Cui, Y.; Thomas, S.; Sutherland, B.; Kleinke, H. *J. Solid State Chem.* **2008**, *181*, 2024–2030.
(39) Kittel, C. *Introduction to Solid State Physics*, 7th ed.; John Wiley & Sons: New York, 1996; p 166.
(40) Snyder, G. J.; Christensen, M.; Nishibori, E.; Caillat, T.; Iversen, B. B. *Nat. Mater.* **2004**, *3*, 458–463.
(41) Sales, B. C.; Chakoumakos, B. C.; Mandrus, D.; Sharp, J. W. *J. Solid State Chem.* **1999**, *146*, 528–532.